

# HYBRID NEP-CHEMICAL VEHICLE AND PROPULSION TECHNOLOGY STUDY FOR CREWED MARS MISSIONS

Mathew Duchek, Matteo Clark, Alejandro Pensado, Christopher Harnack, William Machemer,  
Emanuel Grella and Min Qu

Analytical Mechanics Associates, Inc.  
Denver, CO

## ABSTRACT

Nuclear Electric Propulsion (NEP) is a suite of technologies with the potential to enable crewed opposition-class missions to Mars. Each subsystem comprising an NEP system has multiple technology options that present tradeoffs in vehicle sizing and technology development risk. Multiple vehicle concepts have been studied in the past and are currently being studied at NASA.

Three models have been developed to illustrate the impact of key technology parameters on overall sizing for a crewed Mars transportation vehicle. Vehicle mass required to close the mission as a function of NEP system alpha ( $\text{kW}_e/\text{kg}$ ) and specific impulse ( $I_{sp}$ ) is estimated with a detailed trajectory model. A power system mass model estimates alpha as a function of power and radiator mass assumption. A power conversion system thermodynamic model predicts the radiator area required to close a Brayton cycle power conversion system. Combined with the architecture mass required for mission closure, the radiator area and alpha model provide insight into how technology development may impact the mission. Our focus is on parametric sweeps of the whole design space rather than any particular point design. Results from the mission model comparing electric propulsion technology (Hall, Ion, Magnetoplasmadynamic) and both 2039 and 2042 opposition-class mission launch windows are included.

The results of the study illustrate the technology parameters that can result in mission closure and illustrate where the architecture is sensitive to variations in technology performance or requirements.

## INTRODUCTION

NASA is investigating options for sending humans to Mars within the next 20 years. A key system to enable such a mission is the propulsion system for the deep space transport. Nuclear Electric Propulsion (NEP) is one option for the primary propulsion. A NEP system is composed of a number of key technologies including a reactor, a power conversion system, thermal radiators, and electric thrusters. The performance of each of these technologies can have a significant impact on the scale of vehicle needed to enable a crewed Mars mission. This paper describes an effort to parametrically model the key technologies of a NEP system to show the impact of their performance on the size and mass, and thus feasibility, of the transport vehicle.

Three models with various degrees of interconnection form the parametric model set:

- Mission model
- Power conversion model
- Power system mass model

The mission model includes a parametric sizing equation and a trajectory model in Copernicus [1]. The parametric sizing equation predicts the mass of the NEP/chemical vehicle as a function of the power level and the  $\Delta V$  requirement determined by the trajectory model. The trajectory model optimizes the vehicle power and NEP/chemical  $\Delta V$  split to minimize Earth departure mass.

The power conversion model predicts performance of a Brayton cycle power conversion system and the required radiator area as a function of a range of technology choices and performance assumptions. This model is linked to the power system mass model so that power

system specific mass ( $\alpha$ ) estimates can be made as a function of the power conversion technology assumptions.

The power system mass model estimates the mass of the primary components of the NEP power system as a function of power level. This provides a build-up of  $\alpha$  in terms of kg/kW<sub>e</sub>. A block diagram illustrating the boundaries of each model and what is included in the definition of  $\alpha$  is provided in Figure 1.

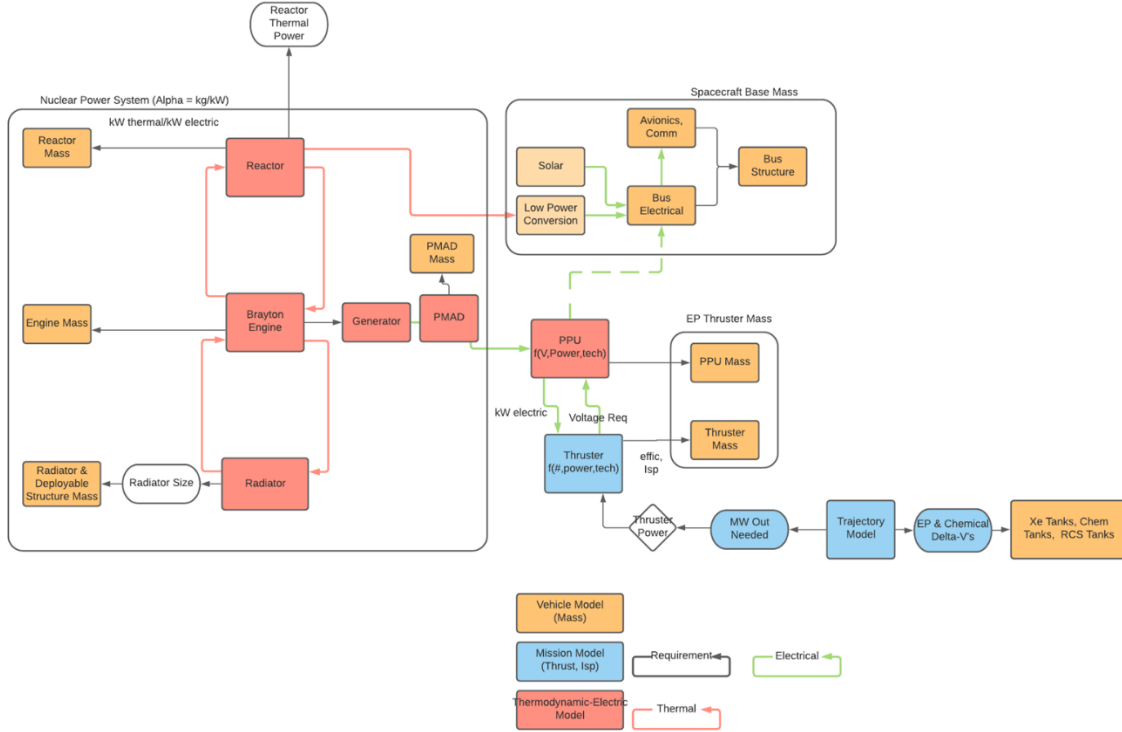


**Figure 1. Parametric Model Block Diagram.**

## MISSION DESIGN

A NEP/chemical hybrid propulsion trajectory optimization tool [2] was used to understand the effect of technology and trajectory assumptions in the context of a crewed Mars mission. The focus of this analysis was to evaluate the impact of several key performance parameters on the initial mass (at Earth departure) of the interplanetary vehicle. The evaluated performance parameters include propulsion technologies (Hall, Ion, and MPD thrusters), power system technology performance (in terms of  $\alpha$ ), parametric vehicle mass sizing model inputs, and the Mars mission opportunities and trajectory phasing (2039 vs 2042).

### ASSUMPTIONS AND METHOD

This section will present the assumptions used to define the elements within the models and show how these models fit together to solve the problem at hand.

#### *Propulsion Technologies*

This study evaluated the impact of the following propulsion technologies on a crewed Mars mission: Hall, Ion, and MPD thrusters. The performance of the propulsion technologies considered in this analysis defined by characteristic specific impulse ( $I_{sp}$ ) ranges (shown in Table 1) and efficiency models (shown in Figure 2).

**Table 1. Characteristic  $I_{sp}$  Ranges for each of the evaluated Propulsion Technologies.**

Propulsion Technology	$I_{sp}$ (s)	
	Lower Bound	Upper Bound
Hall Thruster	1000	3500 [3]
Ion Thruster	2500	6500 [4]
MPD Thruster	4000	7000 [5]

The efficiency for each of the propulsion technologies models were developed based on subject matter experts. The models represent the amount of kinetic energy extracted from a thruster per unit of input energy. To gain a better understanding of the impact of  $I_{sp}$ , in particular, a generalized technology-independent set of cases were run with a conservative efficiency of 0.535 (as shown in Figure 2).

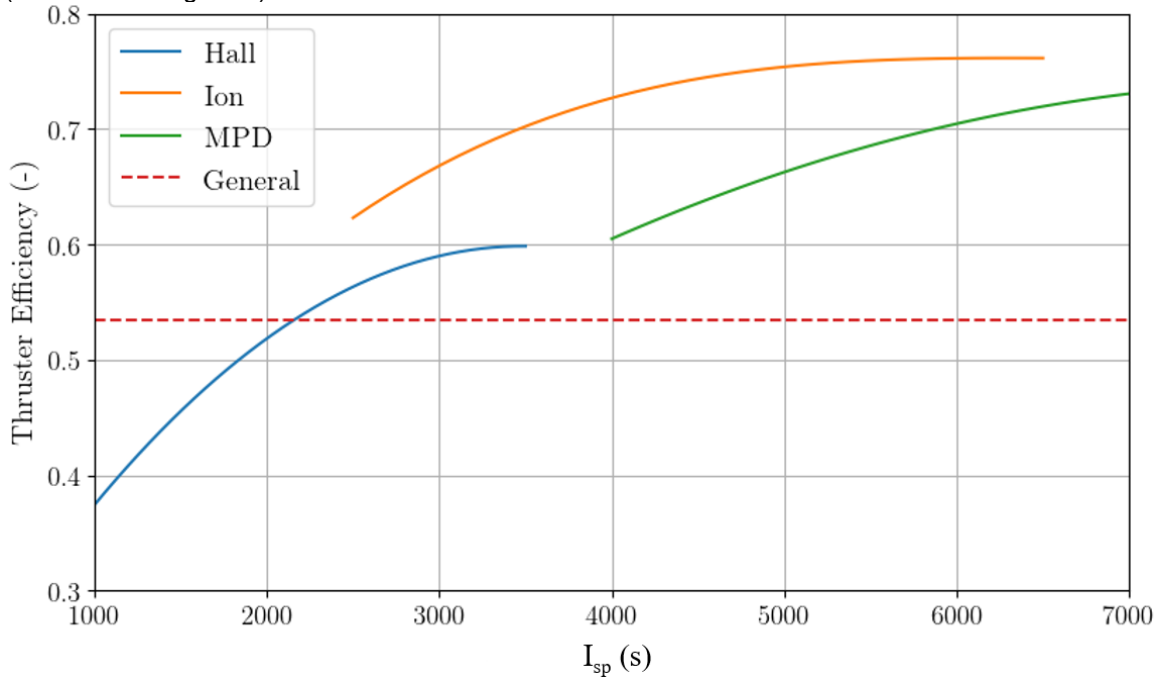


**Figure 2. Thruster Efficiency Comparison for the evaluated Propulsion Technologies [3] [4] [5].**

#### Power System Technology Performance

The spacecraft power system was implemented in the trajectory analysis as a performance parameter range. The inverse specific power (kg/kWe), referred to as  $\alpha$ , defines the mass of the power system for each unit of power required of it. Values of  $\alpha$  between 2 and 30 were assessed within this study.

#### Vehicle Mass Model

The mission vehicle is parametrically sized within the analysis loop based on a system of two equations (Equation 1 and Equation 2). This study evaluated a single set of mass model coefficients (shown in Table 2) derived from first principles representing a more aggressive vehicle mass assumption. As shown in Table 2, the index three parameter is  $\alpha$ , which is appropriately labeled 'variable' given the nature of this trade study.

$$m_{sc} = C_1 + C_2 n_{EP\ engines} + C_3 P_{BOL} + C_4 F_{Thrust} + C_5 n_{chem\ engines} + C_6 m_{prop,EP} + C_7 m_{prop,chem} + C_8 m_{habitat,dry} + C_9 m_{logistics} + C_{10} m_{prop,RCS} \quad \text{Equation 1}$$

**Table 2. Mass Model Coefficients for Equation 1 derived from first principles.**

Index	First Principles Case		Notes
	Constant (C)	Units	
1	23,000	kg	Spacecraft base mass
2	315	kg	EP thruster mass
3	<i>variable</i>	kg/kW <sub>e</sub>	Nuclear power system $\alpha$
4	0.001	kg/N	Inverse specific thrust of chemical propulsion system
5	-	kg	Chemical propulsion system unit mass – not used
6	0.04	kg/kg	EP propellant tank mass factor
7	0.03	kg/kg	Chemical propellant tank mass factor
8	0.05	kg/kg	Habitation module mass factor
9	0.05	kg/kg	Logistics storage mass factor
10	0.03	kg/kg	RCS propellant tank mass factor

$$m_{logistics} = C_1 * duration + C_2$$

**Equation 2**

**Table 3. Logistics Mass Model Coefficients for Equation 2**

Index	Constant (C)	Units	Notes
1	11.11	kg/day	Daily logistics consumption rate
2	0	kg	Logistics base mass
-	40	days	Logistics contingency

To get the coefficients and exponents for the first principles tank masses, assumptions are made about the pressure, composition, and shape of the tank. The tank is then sized to fit these requirements for a range of propellant masses. An exponential curve fit is then applied to determine the coefficients and exponents to be used in the mission modeling. This section details the assumptions used in this analysis.

The EP propellant tank was assumed to contain Xe at a pressure of 1210 psi and a temperature of 300 K. The EP propellant is assumed to be split up equally into 3 tanks. This analysis is tied to a minimalist spacecraft structure where the tanks act as the primary spacecraft structure. The tank is assumed to be cylindrical with a length of 2 times its diameter and a 2:1 semi-elliptical dome. The tank is composed of an aluminum liner and wrapped carbon fiber providing the structure. The liner is 0.05 in thick [2] and the carbon fiber is assumed to be quasi isentropic with an effective tensile strength of 2.4 GPa (reflecting an optimum wrapping of the carbon fiber) [3] [4]. There is also assumed to be a steel head on the tank having approximate mass of 5 kg. Since the EP propellant will not be cryogenic, no insulation or thermal management mass was included. A factor of safety of 1.5 and a 33% growth allowance was used to compute the final mass of the tank. There is a significant decrease in tank mass from the conservative case. This comes from a more optimized tank design and neglecting other masses that will scale with tank size such as thermal control, RCS, structures. The mass scaling for the EP tank does not significantly change if more or fewer tanks are used to store the EP propellant.

For the chemical tank, we assume an areal density of 10 kg/m<sup>2</sup> for the tank with an additional 7 kg/m<sup>2</sup> added to account for the insulation and thermal control systems required to maintain the cryogenic propellant in liquid form. A 30% factor is added to account for pressurization systems and secondary structures. A 15% mass growth allowance and a 50% margin are added for any other unknowns. The resulting scaling is calculated to be 0.03 ( $m_{tank}/(m_{propellant})$ ).

### Vehicle Power System

The vehicle's power system within the simulation is an optimization parameter that links the impact of the power technology performance parameter to the propulsion technology for the defined trajectory and vehicle mass model assumptions. The total spacecraft power required can be sub-divided into two parts: 0.2 MW of power for spacecraft systems and the optimized remainder for the propulsion system.

### Mars Mission Opportunities

This study looked at the 2039 and 2042 Mars opposition class missions; the trajectory concept of operations for both opportunities are shown in Figure 3. Each segment within the trajectory concept of operations is described in Table 4, including details about the allocation of the spacecraft's two propulsion systems to specific maneuvers and burns. The differences in both mission opportunity trajectory types, Earth-Mars-Venus-Earth (EMVE) and Earth-Venus-Mars-Earth (EVME), are highlighted in Table 5.

In both mission opportunity cases, the spacecraft initial and final orbit is a near-rectilinear halo orbit in cislunar space. At Mars, the spacecraft inserts into a 5-Sol Mars Orbit, from where the 50-day Mars surface mission departs and returns. A Venus Gravity Assist (VGA) is performed on either the inbound leg of the trajectory (in the 2039 mission opportunity case) or the outbound leg (in the 2042 case). From cislunar departure to cislunar return, the mission duration is constrained to 730 days.

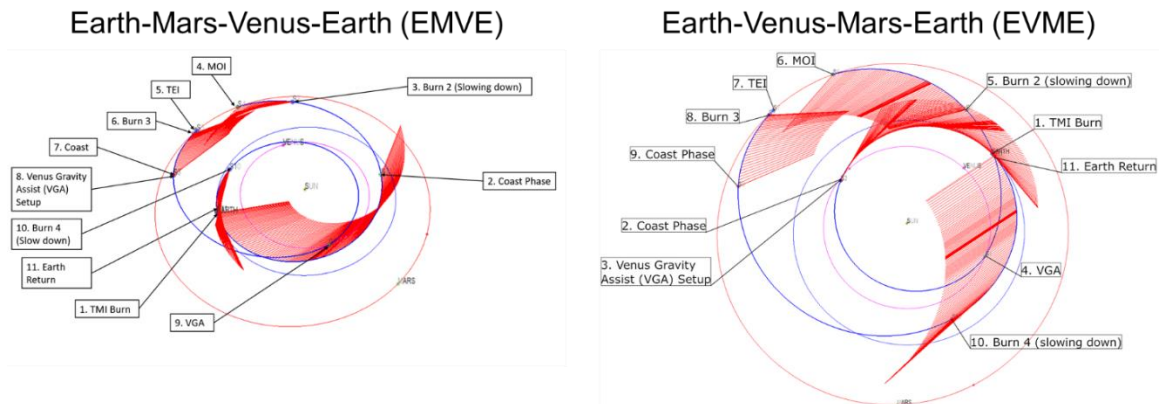


**Figure 3. Trajectory Concept of Operations for Mars 2039 (left) and 2042 (right) opportunity.**

**Table 4. Names and Descriptions of the Modeled Trajectory Segments.**

Segment Name	Segment Description
Trans-Mars Injection (TMI) Burn	An impulsive chemical burn followed by an NEP burn to depart from cislunar space
Coast Phase	An unpowered coast phase between propulsive maneuvers
Mars Approach Burn	An NEP burn to decelerate the vehicle as it approaches Mars
Mars Orbit Insertion (MOI) Burn	A chemical burn to maneuver the spacecraft into a 5-sol Mars orbit
Trans-Earth Injection (TEI) Burn	A chemical burn to maneuver the spacecraft out of a 5-sol Mars orbit
Mars Departure Burn	An NEP burn to accelerate the vehicle away from Mars
Venus Gravity Assist Setup	An unpowered Venus Gravity Assist approach segment
Venus Gravity Assist	An unpowered Venus fly-by
Earth Approach Burn	An NEP burn to decelerate the vehicle as it approaches Earth
Earth Return Burn	A chemical burn to insert the vehicle into an orbit in cislunar space

**Table 5. Comparison of Segment Sequencing between both Mission Opportunity Types.**

EMVE Segment Sequence			EVME Segment Sequence	
1	Trans-Mars Injection Burn	↔	1	Trans-Mars Injection Burn
2	Coast Phase	↔	2	Coast Phase
3	Mars Approach Burn	↔	3	Venus Gravity Assist Setup
4	Mars Orbit Insertion Burn	↔	4	Venus Gravity Assist
5	Trans-Earth Injection Burn	↔	5	Mars Approach Burn
6	Mars Departure Burn	↔	6	Mars Orbit Insertion Burn
7	Coast Phase	↔	7	Trans-Earth Injection Burn
8	Venus Gravity Assist Setup	↔	8	Mars Departure Burn
9	Venus Gravity Assist	↔	9	Coast Phase
10	Earth Approach Burn	↔	10	Earth Approach Burn
11	Earth Return Burn	↔	11	Earth Return Burn

## MISSION DESIGN RESULTS

### *Overview of Results*

As a baseline, several propulsion technology-agnostic sets of cases were run. As was defined in the Propulsion Technologies section, the electrical power to thrust conversion efficiency for these generalized cases was set at 0.535. Fixing this efficiency reduced the complexity of the models, which was beneficial when exploring the data and understanding the interactions between the vehicle sizing and trajectory optimization. An example output from these generalized cases is shown in Figure 5, where the impact of NEP  $I_{sp}$  (the x-axis) and power system  $\alpha$  (the y-axis) on the spacecraft initial mass are visualized. Regions within the plot area that are not filled with a color are regions where architecture closure was not achieved. Alternately, regions that are filled with a color indicate that a feasible solution was identified. Red lines, labeled A and B, are superimposed over the figure to highlight the boundary between regions where architecture closure was achieved and those where it was not. An arrow is also included to indicate the general direction (along the x- and y-axis) that would result in a lower initial vehicle mass.

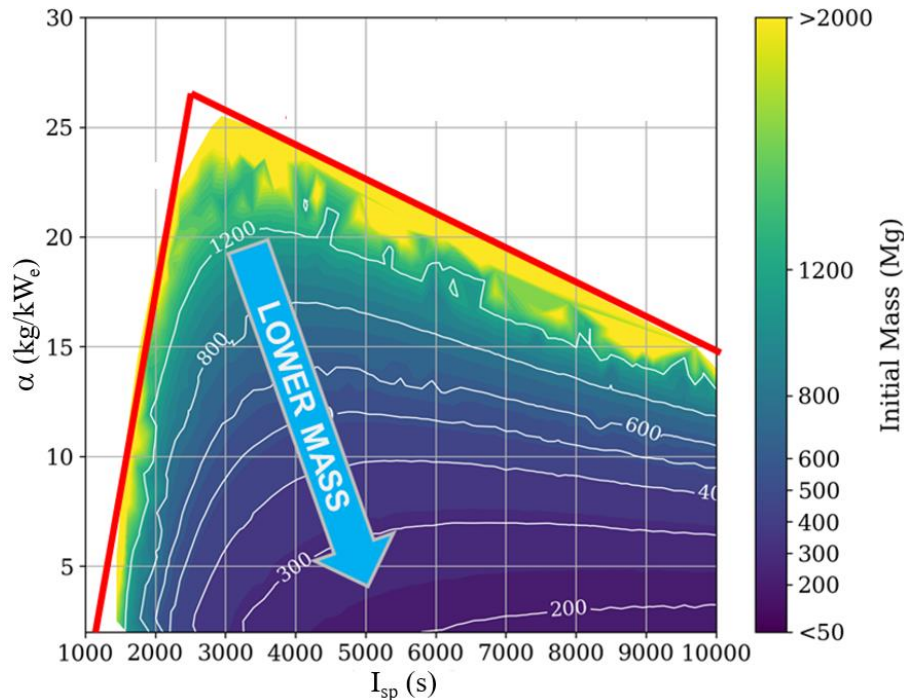


**Figure 4. Generalized case showing impact of NEP  $I_{sp}$  and power system  $\alpha$  on the initial vehicle mass. Trajectory closure is not achieved in the white areas of the plot.**

In assessing the entire data set behind the generalized case shown in Figure 4, it was determined that the spacecraft's thrust-to-weight ratio ( $T/W$ ) is the factor that drives trajectory optimization and architecture closure. The architecture does not achieve closure when the combination of vehicle and trajectory do not meet their defined constraints, typically due to unsustainable mass growth of the vehicle.

The power system  $\alpha$  plays a significant role in the definition of boundary A. For a constant specific impulse, an increase in  $\alpha$  leads to an increase in the mass of the power system and that reduces  $T/W$ . With a lower  $T/W$ , either a longer NEP burn duration or an increase in the NEP thrust level or more reliance on chemical propulsion are required to compensate. In reality, a combination of the three occurs each resulting in a further reduction in the  $T/W$  and further unsustainable vehicle growth. Boundary A occurs at the point where there is no further time available to allocate to NEP burns and as a result, the trajectory will no longer close.

Boundary B is defined by the unsustainable propellant mass growth. As the  $I_{sp}$  of the EP system decreases, more propellant is needed to provide the required delta-V. The optimal split between EP and chemical also trends toward more reliance on the chemical propulsion system as the difference in  $I_{sp}$  between the systems is less. The  $T/W$  also decreases, as mass increases faster than thrust as  $I_{sp}$  decreases. Moving to lower  $I_{sp}$ , the delta-V required eventually exceeds what the chemical propulsion can provide with its  $I_{sp}$  and available propellant mass fraction, and the architecture no longer closes.

Note that the constant value contour lines within Figure 4 (and subsequent figures) are smooth and regular in the regions where the spacecraft initial mass is at its lowest. As a given set of assumptions yields solutions that approach the non-closure region, the optimization problem becomes much more unstable and leads to the more jagged contour lines in the results.

#### *Mission Opportunities (2039 v 2042)*

Two mission opportunities were evaluated with the general thruster efficiency assumption, 2039 EMVE and 2042 EVME. The results are shown in Figure 5. The figure shows that for the same range in NEP  $I_{sp}$ , power system  $\alpha$ , and vehicle mass model assumptions, the 2042 opportunity yields significantly more feasible architectures. The reason for this difference is the trajectory geometry; there is a Venus gravity assist on the outbound leg of the trajectory (when the

vehicle is more heavily loaded) and more lead-time to conduct NEP burns. These factors result in a reduction in the propulsion power level, subsequently decreasing the mass of the vehicle and therefore increasing the T/W. This trend is observed in the propulsion technology-specific cases and vehicle mass sizing model cases that were run.

For the equivalent cases and assumptions, the spacecraft power level is shown in Figure 6. The first thing to note is the increase in contour line irregularity. This is because the spacecraft power level is an optimization variable (not the optimization objective as is the case for the spacecraft initial mass) and because the model is not very sensitive to variations in mass. A noteworthy trend can be seen in the right sub-plot of Figure 6, where there is a step-like threshold between  $\alpha$  values of 10 and 18-20 kg/kW; below this threshold, more reliance is placed on the NEP system, whereas above the threshold, the spacecraft is optimized to use more chemical propulsion.

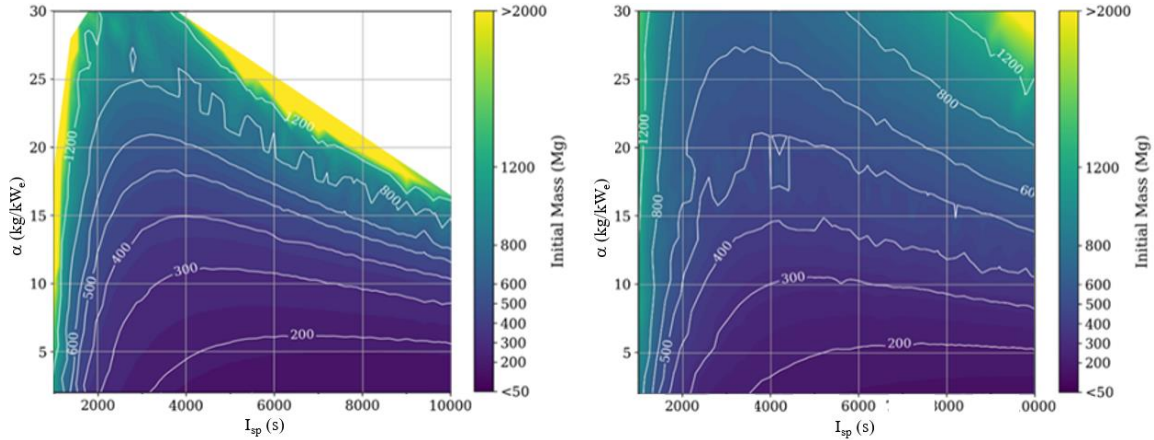


**Figure 5. The initial spacecraft mass for both evaluated mission opportunities (left: 2039-EMVE and right: 2042-EVME).**

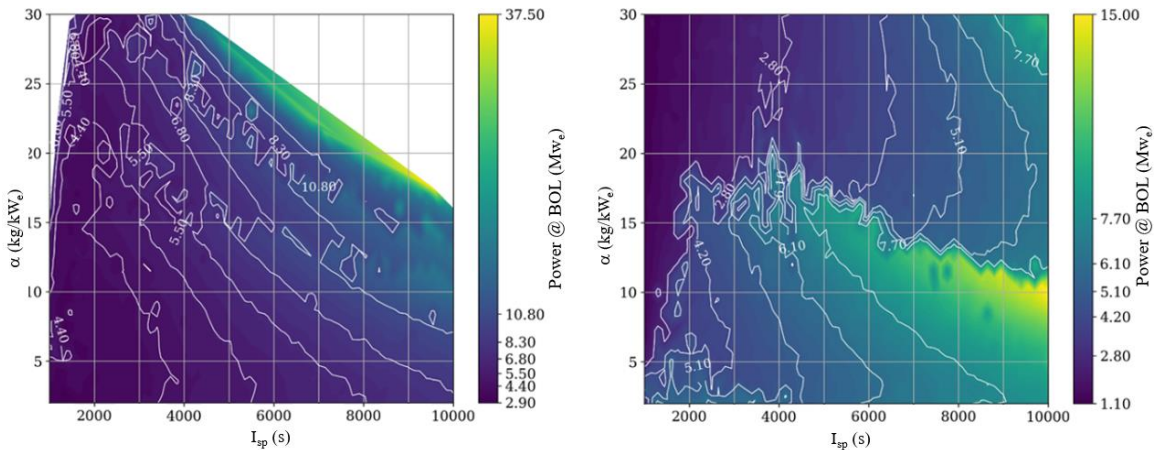


**Figure 6. The spacecraft power level at Beginning-Of-Life (BOL) for both evaluated mission opportunities (left: 2039-EMVE and right: 2042-EVME).**

### Thruster Types

A comparison of the three propulsions technologies (Hall, ion, and MPD thrusters) was evaluated as part of this project; the results are shown in Figure 7.

The Hall thruster had the worst performance in terms of both the initial vehicle mass and architecture closure. This can be attributed to the lower thrust efficiency as well as the lower  $I_{sp}$  range capability. The ion and MPD thrusters both close the architecture over a wider range of their operational capability, but the ion thruster type has a better initial mass performance due its higher thruster efficiency for a given  $I_{sp}$ .

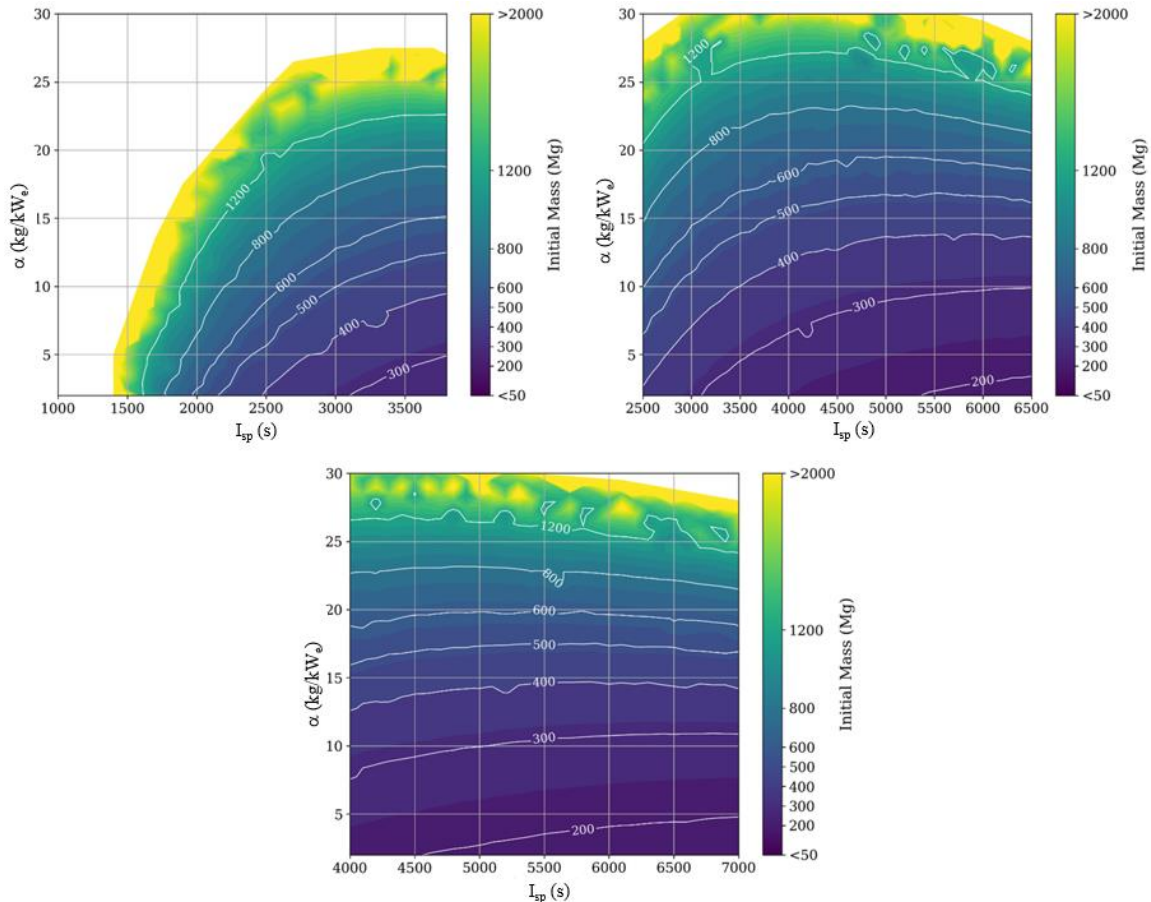


**Figure 7. Initial Vehicle Mass comparison between the Hall (left), ion (right), and MPD (bottom) thrusters for the same mass model assumptions and the 2039 mission opportunity.**

## DISCUSSION

The most significant initial mass sensitivity examined is in the launch opportunity, particularly in phasing of the Venus fly-by. A Venus fly-by on the outbound leg of the trajectory allows the spacecraft to thrust for longer at a point in time where its thrust-to-weight ratio is at its worst. While one option performs better than the other, the lower performance option cannot be discarded; stakeholder requirements could impose the need for both mission opportunity types and subsequently drive technology development decision-making.

The primary performance indicator for different thruster types is their efficiency and their  $I_{sp}$  range. The present results indicate that efficiency might be a more important parameter than the  $I_{sp}$ . As it stands, the efficiency of ion thruster leads it to be the propulsion technology type enabling the lowest initial mass vehicle for the analyzed mission and mass assumptions.

## POWER CONVERSION MODELING

### Overview and Capabilities

The purpose of the Brayton cycle model is to calculate the thermodynamic state points and power levels of the components within a Brayton cycle, and use this information to understand the impact of system-level design decisions on the system's mass and performance. As the radiator area is a significant portion of the mass of a NEP vehicle [6], investigating how the technology selection and cycle conditions effect the radiator area is a primary objective. Past work from [7], [8], and [9] was used during the development of the model.

The Brayton cycle model, developed in Simulink [10], can calculate the state points and power levels of a closed steady state NEP Brayton cycle for He-Xe and CO<sub>2</sub> working fluids, with the ability to operate with various fluids found within the CoolProps thermodynamic library [11]. The model's results have been benchmarked against a He-Xe cycle from Sandia National Labs [12] and agree to within 5%. The current configuration of the model uses the following inputs and outputs as shown in Table 6.

**Table 6. Closed Brayton Cycle Inputs and Outputs**

Model Input	Model Output
Turbine Inlet Temperature	System States (Temperature, Pressure, Mass Flow Rate)
Radiator Outlet Temperature	Component Power Production/Consumption
Produced Electrical Power	Radiator Area
Turbomachinery Efficiencies	Converter Thermal Efficiency
Turbomachinery Pressure Ratio	
Recuperator Effectiveness	
Radiator Properties and Environment	
Compressor Outlet Pressure	
System Pressure Losses	
System Thermal Losses	

The number of independent fluid loops in a Brayton cycle is an area of interest as this allows components like the reactor and radiators to operate with a different working fluid and pressure as the Brayton cycle. Versions of the model with two and three fluid loops have been developed and will be used in future work.

The thermodynamic processes within the model are simplified to not be constrained to any particular hardware or technology. The turbine and compressor are assumed to operate with a fixed isentropic efficiency. The recuperator and heat exchangers follow an NTU-based calculation method [13]. The radiator contains a loop which numerically integrates the thermal heat rejected as a function of the temperature of the fluid as it changes while flowing through the radiator and halts once the radiator outlet temperature matches the user-defined value. The amount of radiator area required for this process is summed throughout the integration and is an output of the radiator subsystem. The assumptions related to the radiator are listed in Table 7.

**Table 7. Example Model Assumptions**

Example Model Assumptions	
Turbine Efficiency	0.85
Compressor Efficiency	0.8
Alternator Efficiency	0.92
Recuperator Effectiveness	0.85
Radiator Emissivity	0.85
Radiator View Factor	0.85
Radiator Sink Temperature	4K
System Pressure Losses	2%
System Thermal Losses	10 kW <sub>th</sub>

The reactor is modeled as a “black box” heat source which raises the temperature of the fluid to the user-specified reactor output temperature and calculates the required thermal power. The alternator subsystem is used to account for losses during the conversion from rotational work to electrical power. Once the net electrical work is calculated, this is divided by the thermal work of the reactor to determine the thermal efficiency of the converter system. To simplify the model, thermal and pressure losses are summed over the entire loop and applied before the reactor and compressor, respectively.

#### *System Temperature Bounds and Radiator Area for He-Xe*

The technology chosen for the Brayton cycle will affect the maximum and minimum temperatures allowable in the cycle. These temperature bounds influence the thermal efficiency and radiator area and is therefore a topic of interest. Each maximum and minimum cycle temperature pair has an optimal pressure ratio that results in the highest thermal efficiency. The model was used to find this optimal pressure ratio by running through a range of pressure ratios and then selecting the pressure ratio of maximum thermal efficiency. Shown in Figure 8 is the range of thermal efficiencies when an input of 1150 K for the turbine inlet temperature and 400 K for the radiator outlet is used. Once the optimal pressure ratio is determined for each temperature pair, this value can be used in the model to generate a radiator area.

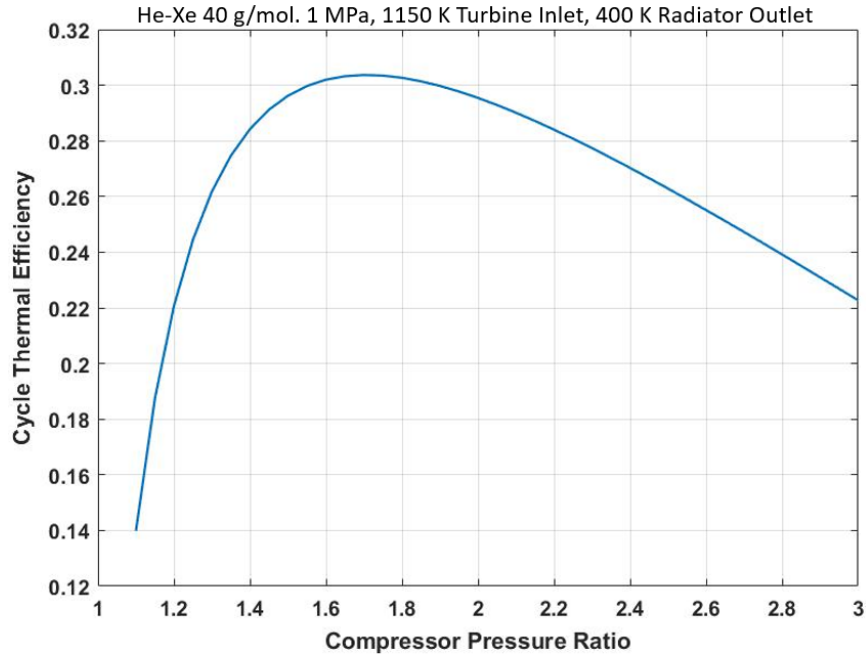


**Figure 8. Pressure Ratio and Thermal Efficiency Effects**

A wide range of turbine inlet temperatures and radiator outlet temperatures were investigated, and the radiator area for each temperature bound was plotted. Figure 9 shows the results for a He-Xe cycle as the radiator area per megawatt of electrical power generated. The turbine inlet and radiator outlet temperatures are set as inputs within the model for each radiator area data point. The radiator size is calculated as an output based on the area needed to reject the amount of heat required to reach the defined outlet temperature.

Each data point in this figure assumes the turbomachinery is operating at the pressure ratio that maximizes thermal efficiency for the given radiator outlet temperature and turbine inlet temperature. Areas within the plot with no color are regions where the model did not thermodynamically close. Figure 10 is the identical plot but with the thermodynamic efficiency of the cycle displayed as contour lines.

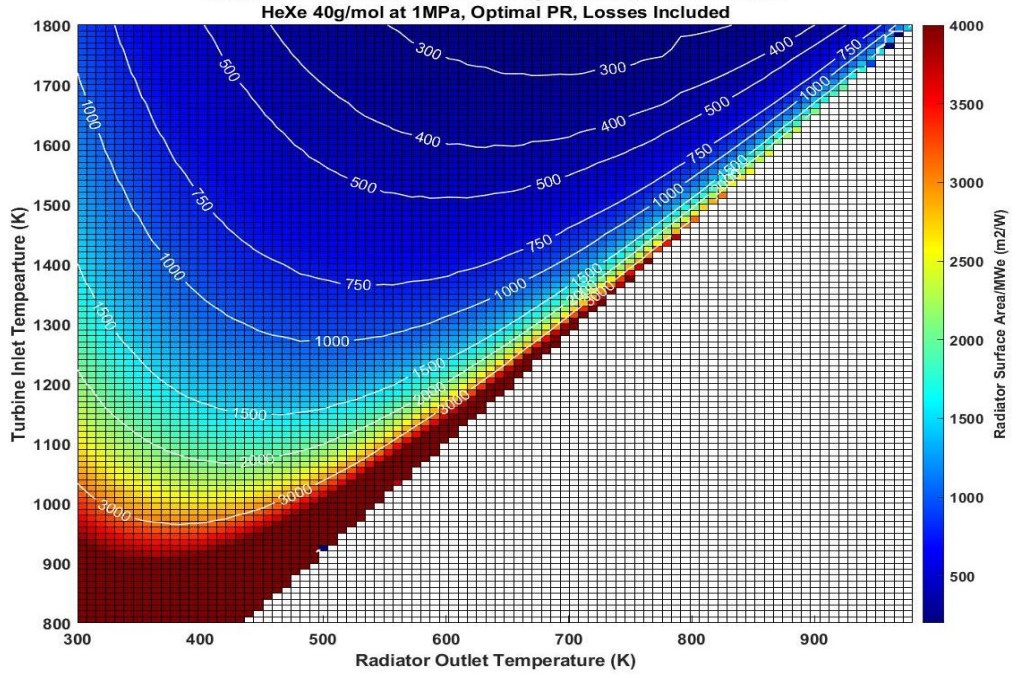


Figure 9. Radiator Area for Various System Temperature Bounds

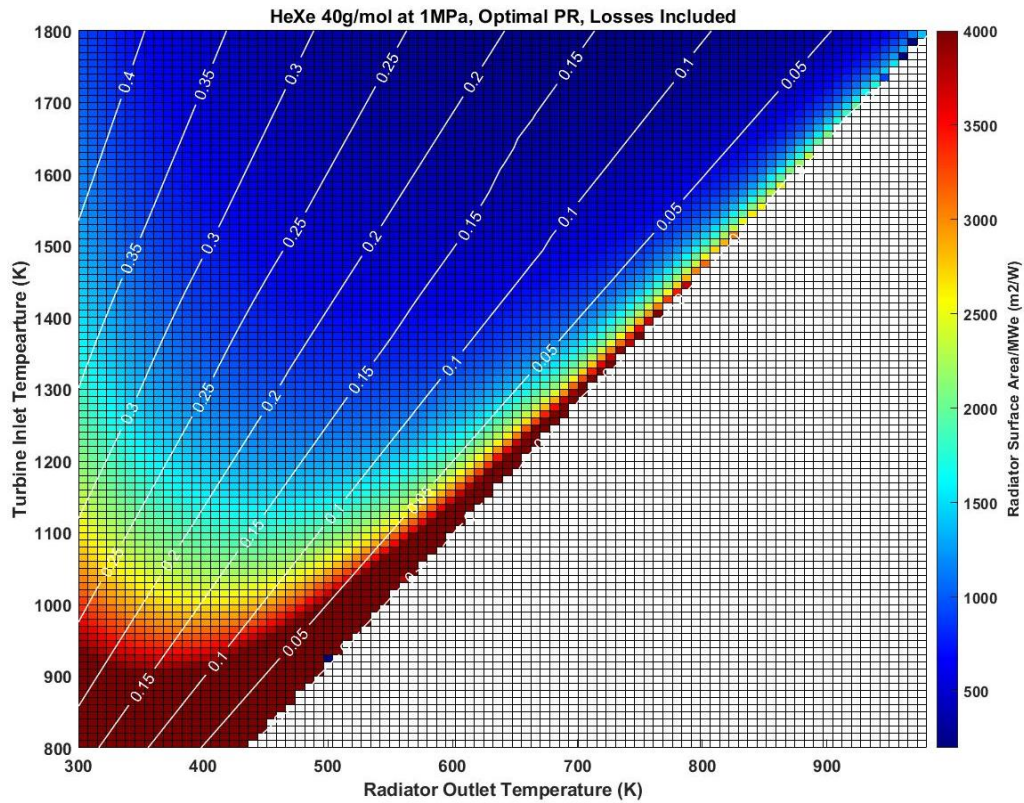


Figure 10. Radiator Area for Various System Temperature Bounds with Thermal Efficiencies

The minimum radiator area for each turbine inlet temperature follows a trend from bottom left to top right of the plot, while the trend of maximum thermal efficiency travels towards the top left of

the plot. The combined differences of these trends result in a minimum radiator area that exists near the middle of the available radiator outlet temperature for each turbine inlet temperature. The minimum radiator area also increases exponentially as the turbine inlet temperature decreases. In these example results, the radiator area slope becomes more gradual above 1200 K turbine inlet temperature and at roughly 485 K radiator outlet temperature.

### HEAT PIPE TECHNOLOGY AND WORKING FLUID

Heat pipes will be a necessary technology to distribute the waste heat across the radiators for any NEP mission. There are a wide variety of fluids that can be used in heat pipes and one of the most important factors in choosing a fluid is the operating temperature of the radiator. Figure 11 shows the temperature ranges of potential heat pipe fluids [14]. The overlaid plot shows the radiator area and the operating conditions of the power conversion cycle. Figure 11 only shows the radiator outlet temperature, but it is important to consider the inlet temperature to the radiator as well, which could be as much as 200 K higher than the outlet temperature. The heat pipe fluid will need to operate over this entire radiator temperature range. This means that some operating conditions are not feasible due to a lack of appropriate heat pipe fluid. Another important observation from Figure 11 is that water heat pipes are the only option at a high technology readiness level for radiator temperatures between 400 K and 600 K. This limits the ability of water heat pipes to minimize radiator area in higher temperature systems. Cesium and cesium mixtures have a lower technology readiness level but warrant more investigation as they would allow for hotter radiator outlet temperatures, and therefore, smaller radiators.

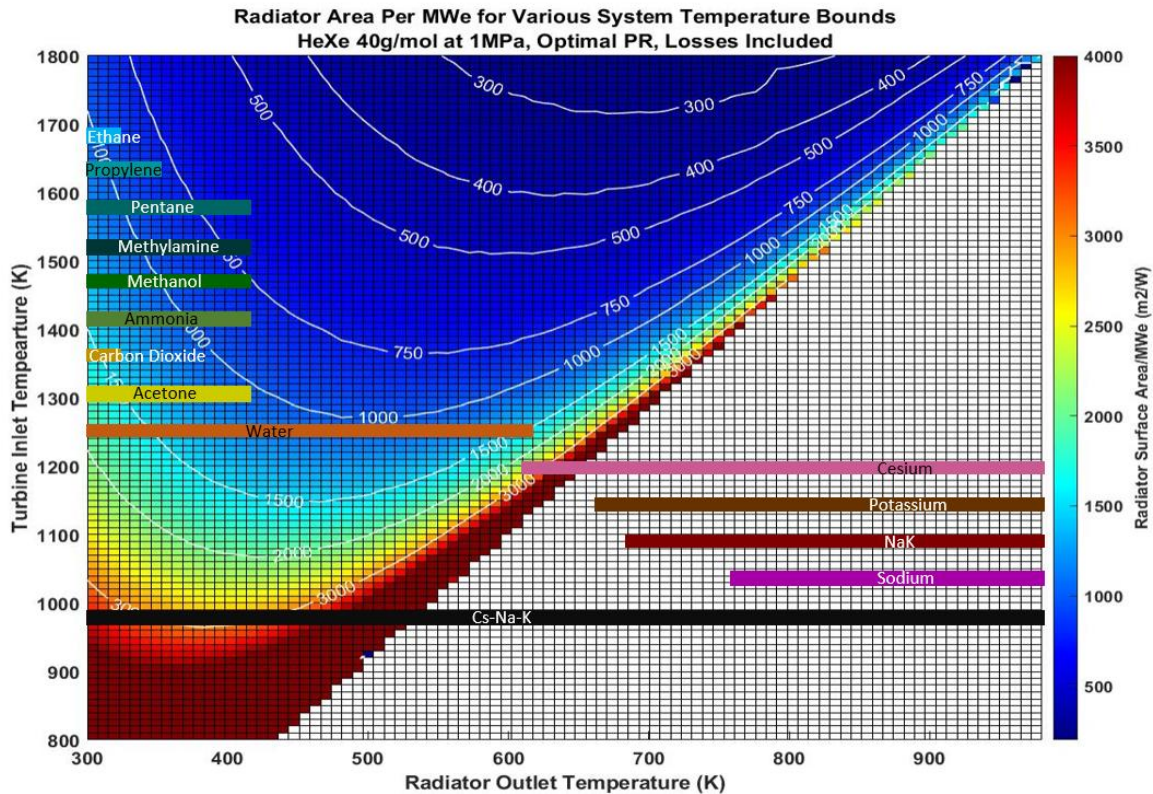


Figure 11. Overlay of the working temperatures of candidate heat pipe fluids.

## SPECIFIC MASS MODELING

The system mass per kW of electric power produced, or  $\alpha$ , is a crucial metric in assessing the validity and feasibility of a NEP vehicle. The power system specific mass model described here represents a first iteration model that estimates  $\alpha$  as a function of system power and power conversion inlet temperature. Such models have been developed by others in the past [15]; our intent was to create a mass model that can be linked to the mission and power conversion models described in this paper and re-generate mass results for a range of different technology assumptions.

Subsystem-level mass estimates are based on curve fits to historical data or estimates from other published work as described below. The exception is the radiator, which is estimated using a mass per area assumption and area calculated with the power conversion model described in the following section.

### *Subsystems Based on Historical Data and Published Studies*

The scaling equations listed below are intended to approximate how the power conversion components scale with power to get a first approximation of the feasibility of different mission architectures. For a higher fidelity approach, it is recommended that a mass model be derived from a first principles approach as was done for the radiator. Note that the “ $\alpha$ ” functions, below, have inversely proportional scaling to the systems electrical power,  $P_e$ .

$$\alpha_{reactor} = P_e^{-0.567} 10^{2.358} \quad \text{Equation 3}$$

$$\alpha_{turbo} = 10.317 P_e^{-0.344} \quad \text{Equation 4}$$

$$\alpha_{recuperator} = P_e^{-1.011} 10^{1.804} \quad \text{Equation 5}$$

$$\alpha_{PMAD} = 128.63 P_e^{-0.502} \quad \text{Equation 6}$$

Equation 3, which represents the reactor’s scaling function, is a fitted scaling function to a neon gas cooled Pylon reactor design at 50 kW<sub>e</sub>, 100 kW<sub>e</sub>, and 1 MW<sub>e</sub> with a 1- $\pi$  steradian radiation shield [7]. This reactor design is representative of the reactor needed for a NEP system and scales with power as expected, though the details of an actual system would likely vary. Equation 4 and Equation 5 were created using components built such as BRU, Mini-BRU, BHXU and design points from researchers [7] [16] [17] [18] [19] [20] [21] [20]. The ducting and structure specific mass was assumed to be 20% of power conversion components’ specific mass. The scaling function of the power management and distribution (PMAD), Equation 6 was developed by Mason [22]. There are two radiators for the PMAD, one to discharge waste heat or PMAD radiator and a parasitic load radiator. Their  $\alpha$  values were found with the following assumptions using the radiator mass model detailed in the next section: the PMAD radiator average temperature and area density were set to 400 K and 7 kg/m<sup>2</sup>, while the parasitic load radiator set to 850 K and 10 kg/m<sup>2</sup>.

### *Heat Rejection Alpha and Radiator Mass Model*

The radiator specific mass model was developed from a first principles analysis of the radiator system. The radiators themselves are assumed to have a particular areal density and the support structure was then sized to accommodate this mass. The area density accounts for the mass of the panels as well as the heat transport system and fluid distributing the heat throughout the radiator. For the plots below, mass per area is assumed to be 7 kg/m<sup>2</sup> [23]. 7 kg/m<sup>2</sup> is less than the current ISS radiators at 8.8 kg/m<sup>2</sup>, but greater than the 5.1 kg/m<sup>2</sup> in the Jupiter Icy Moon Orbiter (JIMO) concept [3].

Sizing the radiator support structure was driven by vibrational loading during launch as well as acceleration loading during the high thrust chemical propulsion portion of a NEP/chemical propulsion Mars transit. We assume here that the radiators will be folded inside a fairing during launch. In this configuration, we assume that the radiator system must have a first natural frequency mode above 5 Hz. During Mars transit the radiator will be fully deployed and will need to withstand an acceleration of 0.66 m/s<sup>2</sup>, the maximum acceleration provided by the chemical

stage of the NEP vehicle. This acceleration is comparable to the firing of two RL-10 class chemical engine with an earth arrival mass of 170,000 kg (the lightest mass of the vehicle under highest thrust). A safety factor of 2 is applied to both calculations and the support structure mass is increased by 5% to account for deployment mechanisms.

When this first-principles estimation of the radiator system mass is combined with the Brayton cycle model, values of the specific mass for the radiator element can be obtained for different operating conditions. Figure 12 shows the radiator system specific mass at different operating conditions. The radiator system specific mass is smaller for higher turbine inlet temperatures due to the higher efficiencies these cycles have. From Figure 13, it can be observed that the specific mass for the radiator panels is constant, as an increase in electrical power leads to a proportional increase in heat rejection capabilities. The reduction in specific mass at higher power levels instead comes from the support structure.

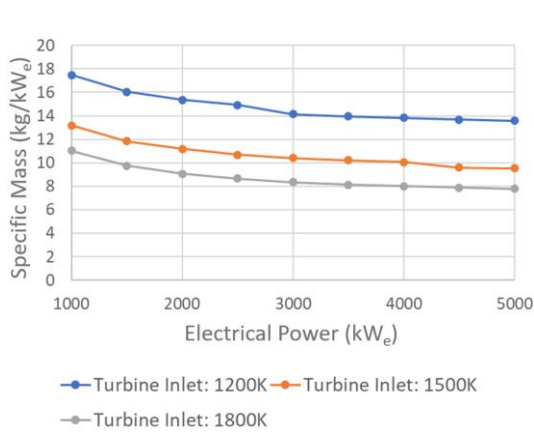


**Figure 12. Radiator system specific mass curve.**

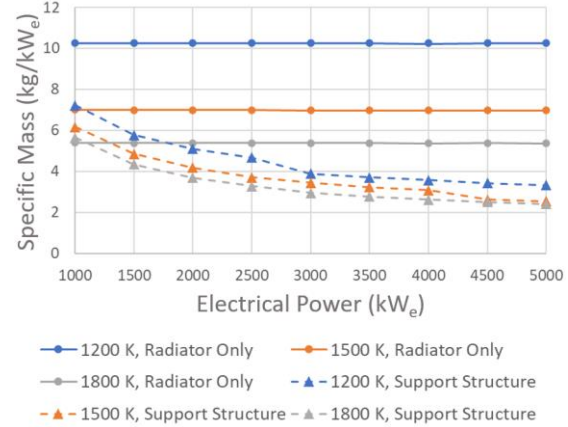


**Figure 13. Specific mass curve breakdown into the radiator and support structure.**

#### Results of the Complete Specific Mass Buildup

The results of the  $\alpha$  model buildup are shown in Figure 14. This buildup assumes a radiator areal density of 7 kg/m<sup>2</sup>, a single-loop system, and four Brayton power converters with one reactor. In this model the heat rejection system takes up most of the mass followed by the PMAD, reactor and power conversion systems. The recuperator mass is small at only 5% of the total power conversion system mass. This compares with other studies such as JIMO where the recuperator accounted for 37% of the power conversion system mass [16]. This is a result of the logarithmic scaling function used and the very low  $\alpha$  value of two data points from Noca and Polk [21]. That work used a very light weight rotary recuperator for their mass buildups which they note would require more study and development before the recuperator can be used for long duration non-terrestrial missions.

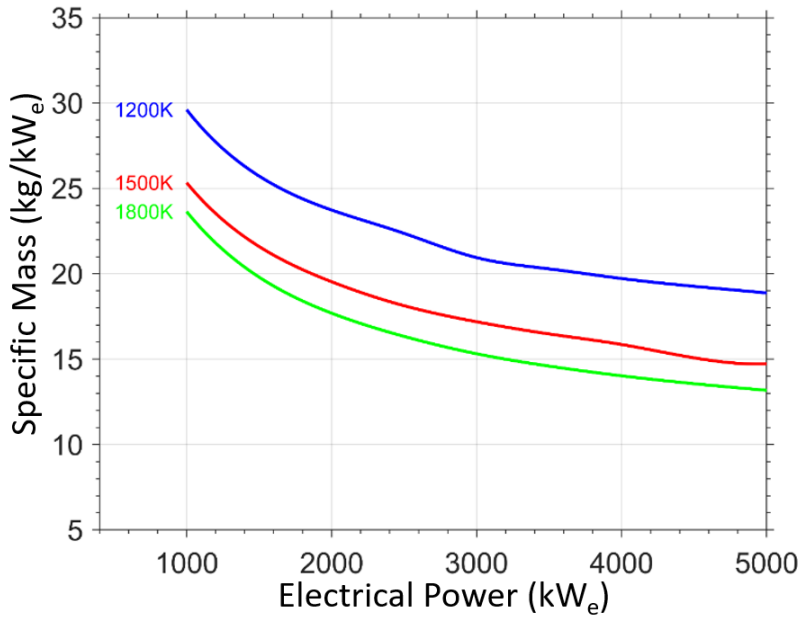


**Figure 14. Complete  $\alpha$  buildup of power conversion system with a radiator areal density of 7 kg/m<sup>2</sup>.**

As shown in Figure 15, the radiator/heat rejection system comprises most of the electrical power system mass. The radiator's required area is driven by the average radiating temperature, but at a given temperature, as in our current model, the mass can vary widely depending on the assumption of areal density of the radiator. Varying this assumption from 3-12 kg/m<sup>2</sup>, we can see in Figure 16 that system  $\alpha$  is sensitive to the assumption of radiator mass per area. The sensitivity is less for cases with higher operating temperatures due to higher thermal efficiency. The heat rejection system's  $\alpha$  percentage will vary between 52% and 86% depending on the assumed areal density of the radiator.

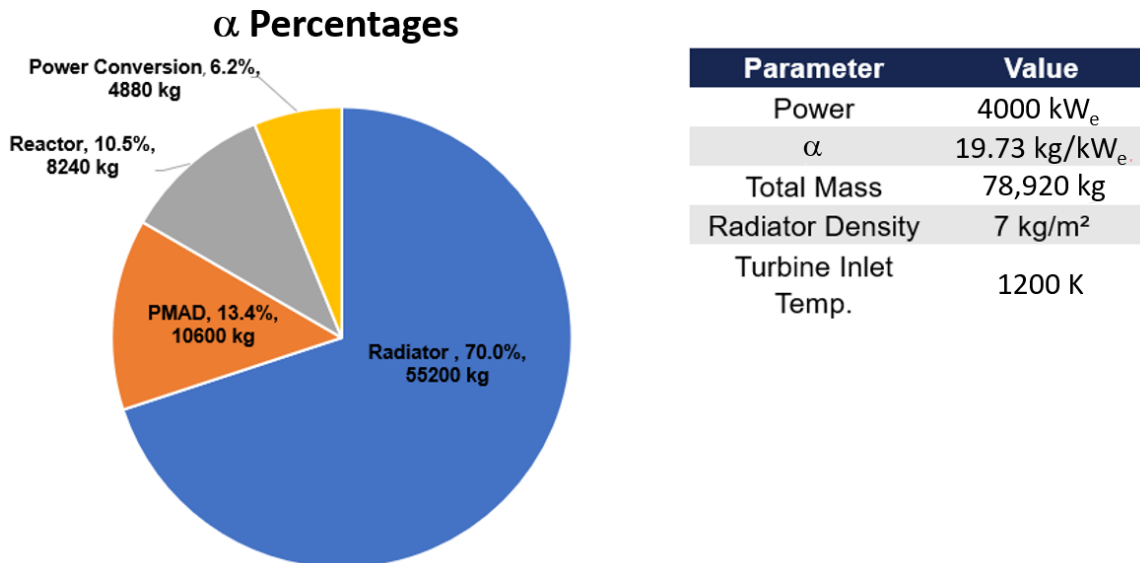


**Figure 15.  $\alpha$  for single loop 4 MW<sub>e</sub> Brayton cycle with 1200 K turbine inlet temperature, a radiator areal density of 7 kg/m<sup>2</sup>, four Brayton converters, and one reactor.**

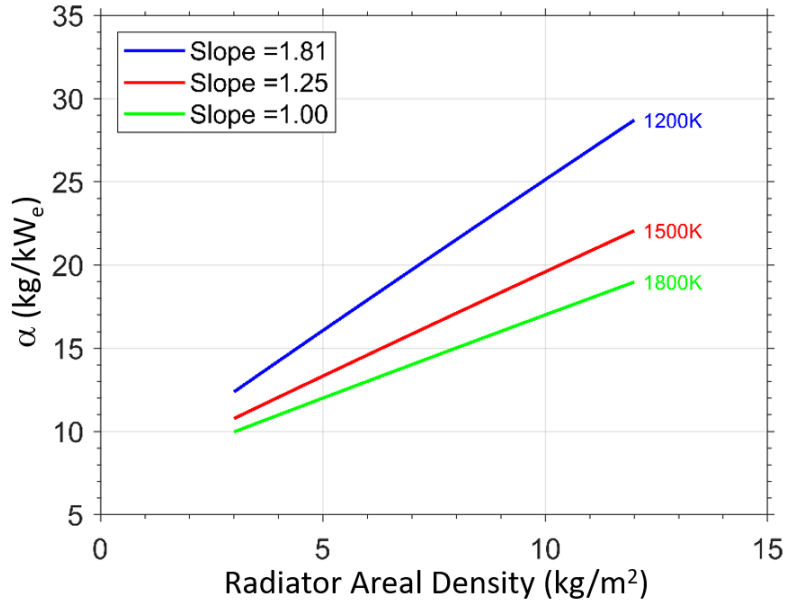


**Figure 16. Relationship between radiator areal density and  $\alpha$  at 4 MW<sub>e</sub> and various turbine inlet temperatures.**

### DISCUSSION

By comparing the results of the three models, the importance of two key performance parameters are evident. First, the cycle maximum temperature has a significant impact on  $\alpha$  via the radiator area, where a higher temperature system has the potential to be a lower mass system (Figure 9). Second, the radiator areal density is a significant driver of  $\alpha$ , as seen in Figure 16. The mission model results in Figure 6 and Figure 7 illustrate the impact of  $\alpha$  on the architecture mass. Figure 17 illustrates the connecting thread from radiator areal mass performance through to architecture mass impact, showing a 3x architecture mass impact over the range of radiator areal density considered.

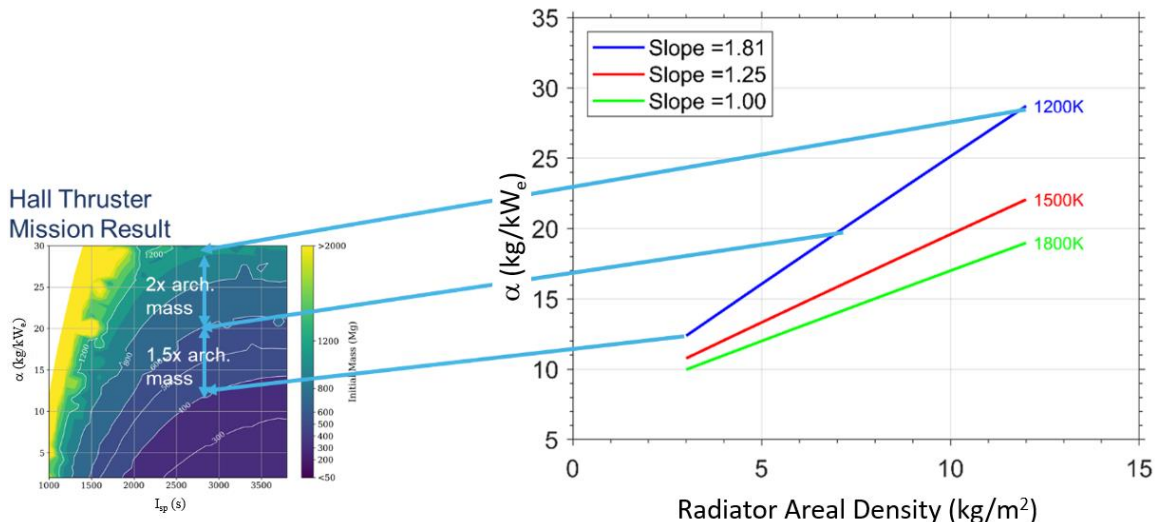


**Figure 17. Impact of radiator area density on architecture mass.**

## SUMMARY AND CONCLUSIONS

Three models covering the mission, power conversion, and power system specific mass have been developed. The trends affecting mission closure as a function of  $\alpha$  and  $I_{sp}$  of the electric propulsion system are illuminated by mission model results. The fundamental tradeoff in power conversion working temperatures, cycle efficiency, and radiator area is explored with the power conversion cycle model. Results of the initial power system mass model illustrate the trend of lowering  $\alpha$  with increasing system power and the strong effect of cycle maximum temperature and radiator specific mass. Continued expansion of these models and investigation of the impacts of technology performance parameters will provide insight into the system-level effects of technology development choices.

## FUTURE WORK

The models described above represent a basic capability to analyze the performance of NEP power systems and their impact on mission vehicle mass. There is much room for adding fidelity to the models and for additional analysis of specific technology options. One area this team continues to work is linking the three models together. A set of technology choices can be used to generate an  $\alpha$  vs. power curve which can serve as a constraint on the mission model for optimizing the power level and architecture mass. Coupling the tools will permit more rapid evaluations of the effects different technology choices have on the overall power system performance and mass. Additionally, sensitivity analysis around the multiple assumptions built into the models would identify which additional performance parameters may drive power system and architecture mass.

For the mission model, future work includes assessing different mission durations to understand how that affects the spacecraft mass and architecture closure. Additionally, further work could include implementing chemical drop stages into the Copernicus trajectory model and evaluating how well vehicles optimized for one opportunity close other mission opportunities. Finally, specific cases corresponding to a particular  $\alpha$  vs. power level curve generated by the alpha model would illustrate the impact of specific technology assumptions on the vehicle mass.

Future work for the Brayton cycle model includes assessing specific technologies including recuperator types, radiator types and heat transfer fluids. This is planned to include CO<sub>2</sub> and He-Xe comparison and higher fidelity input sensitivities.

For the alpha model, future work includes higher fidelity turbomachinery, ducting, and heat exchanger models that will allow for different fluids and operating pressures to be compared.

## ACKNOWLEDGMENTS

Funding for this work was provided by the Space Nuclear Propulsion (SNP) project, managed by Dayna Ise, under NASA contract 80LARC17C0003. Technical direction from the SNP project was provided by Kurt Polzin and Frank Curran.

## REFERENCES

- [1] J. S. C. A. Ocampo, , "The Design and Development of Copernicus: A Comprehensive Trajectory Design and Optimization System", Proceedings of the International Astronautical Congress, IAC-06-C1.4.04, 2006.
- [2] P. R. Chai, R. G. Merrill, K. G. Pfrang and M. Qu, "Hybrid Transportation System Integrated Trajectory Design and Optimization for Mars Landing Site Accessibility," in *AIAA Propulsion and Energy 2019 Forum*, Indianapolis, IN, 2019.
- [3] M. Walker, Interviewee, *K.A. Polzin Personal Communication*. [Interview]. Jan. 2021.
- [4] M. Patterson, Interviewee, *K.A. Polzin Personal Communication*. [Interview]. Jan. 2021.

- [5] V. S. S. A. V. D. G. P. G. Tikhonov, "Research of plasma acceleration processes in self-field and applied magnetic field thrusters," in *IEPC-93-076, 23rd International Electric Propulsion Conference*, Seattle WA, 1993.
- [6] L. S. Mason, "Power Technology Options for Nuclear Electric Propulsion," in *IECEC*, Washington, 2002.
- [7] C. G. Morrison, "Temperature and Power Specific Mass Scaling for Commercial Closed-Cycle Brayton Systems in Space Surface Power and Nuclear Electric Propulsion Applications," in *Nuclear and Emerging Technologies for Space*, Richland, 2020.
- [8] A. Harper, "Study of Reactor Brayton Power Systems for Nuclear Electric Spacecraft," Airesearch Manufacturing Company of Arizona, Phoenix, 1979.
- [9] V. Dostal, M. J. Driscoll and P. Hejzlar, "A Supercritical Carbon Dioxide Cycle for Next Generation Nuclear Reactors," Advanced Nuclear Power Technology Program, Cambridge, 2004.
- [10] "Automatic Code Generation - Simulink Coder," MathWorks, [Online]. Available: <https://www.mathworks.com/products/simulink-coder.html>. [Accessed 28 June 2015].
- [11] I. Bell, J. Wronski, S. Quoilin and V. Lemort, "Pure and Pseudo-pure Fluid Thermophysical Property Evaluation and the Open-Source Thermophysical Property Library CoolProp," *Industrial & Engineering Chemistry Research*, vol. 53, no. 6, pp. 2498-2508, 2014.
- [12] S. A. Wright, R. J. Lipinski, M. E. Vernon and T. Sanchez, "Closed Brayton Cycle Power Conversion Systems for Nuclear Reactors," Sandia National Laboratories, Albuquerque, 2006.
- [13] F. P. Incropera, D. P. Dewitt, T. L. Bergman and A. S. Levine, in *Principals of Heat and Mass Transfer, 7th Edition*, Hoboken, NY, Wiley & Sons, pp. 122-130.
- [14] K. Polzin, *NEP Thermal Management Technical Interchange Meeting*, NASA, 2021.
- [15] L. Mason and D. Jacobson, "Promising Nuclear Electric Propulsion Concepts for Human Mars Missions," in *Future In-Space Operations (FISO) Seminar*, 2020.
- [16] L. S. Mason, "A Power Conversion Concept for the Jupiter Icy Moons Orbiter," in *First International Energy Conversion Engineering Conference*, Portsmouth, 2003.
- [17] L. S. Mason and J. G. Schreiber, "A Historical Review of Brayton and Stirling Power Conversion Technologies for Space Applications," *Space Nuclear Conference*, 2007.
- [18] M. S. El-Genk and B. M. Gallo, "High Performance Brayton Rotating Unit (UNM-BRU-3) for Space Reactor Power Systems," in *7th International Energy Conversion Engineering Conference*, Denver, 2009.
- [19] A. Harper, "Study of Reactor Brayton Power Systems For Nuclear Electric Spacecraft d," Airesearch Manufacturing Company of Arizona , Phoenix, 1979.
- [20] J. D. Duncan, J. C. Gibson, R. F. Graves, C. J. Morse and C. E. Richard, "Brayton Heat Exchanger Unit Development Program (Alternate Design)," Airesearch Manufacturing Company of Arizona, Albuquerque, 1973.
- [21] M. Noca, J. E. Polk and R. Lenard, "Evolutionary Strategy for the Use of Nuclear Electric Propulsion in Planetary Exploration," in *STAIF 2001 (space technology & applications international forum) 18th Symposium on nuclear power and propulsion*, Albuquerque, NM, USA, 2001.
- [22] R. H. Frisbee and R. C. Moeller, "Identification of Mission Sensitivities for High-Power Electric Propulsion Systems," *41st AIAA/ASME/SAE/ASEE Joint Propulsion Conference and Exhibit*, 2005.
- [23] L. Mason, D. Beach and J. Yuko, "Heat Rejection Concepts for Brayton Power," Glenn Research Center, Cleveland, 2005.
- [24] A. C. Marshall, "RSMAS-D Models: An improved Method for Estimating Reactor and Shield Mass for Space Reactor Applications," Sandia National Laboratories, Albuquerque, 1997.

